Origin of NBTI Variability in Deeply Scaled pFETs

B. Kaczer, T. Grasser[1], Ph. J. Roussel, J. Franco[2], R. Degraeve, L.-A. Ragnarsson, E. Simoen, G. Groeseneken[2], H. Reisinger[3]

IMEC, Kapeldreef 75, B-3001 Leuven, Belgium, phone: +32-16-281-557, email: ben.kaczer@imec.be

[1]Christian Doppler Laboratory for TCAD, Institute for Microelectronics, TU Wien, A-1040 Vienna, Austria

[2]also ESAT, KU Leuven, Leuven, Belgium

[3]Infineon Technologies AG, D-81730 Munich, Germany

Abstract*—The similarity between Random Telegraph Noise and Negative Bias Temperature Instability (NBTI) relaxation is further demonstrated by the observation of exponentially-distributed threshold voltage shifts corresponding to single-carrier discharges in NBTI transients in deeply scaled pFETs. A SPICE-based simplified channel percolation model is devised to confirm this behavior. The overall device-to-device ΔV_{th} distribution following NBTI stress is argued to be a convolution of exponential distributions of uncorrelated individual charged defects Poisson-distributed in number. An analytical description of the total NBTI threshold voltage shift distribution is derived, allowing, among other things, linking its first two moments with the average number of defects per device.

Keywords: pFET, Negative Bias Temperature Instability, Random Telegraph Noise, variability, Random Dopant Fluctuations

I. Introduction

The large, micrometer-sized FET devices of the past CMOS technologies were considered identical in terms of electrical performance. Similarly, the application of a given stress resulted in an identical parameter shift in all devices. With the gradual downscaling of the FET devices, the oxide dielectric was the first to reach nanometer dimensions, thus introducing the first stochastically distributed reliability mechanism—the time dependent dielectric breakdown [1]. With the shrinking of *lateral* device dimensions to atomic levels, variation between devices appeared due to effects such as random dopant fluctuation and line edge roughness. Similarly, application of a fixed stress in such devices results in a distribution of the parameter shift. Understanding these distributions will be crucial for correctly predicting the reliability of future deeply downscaled technologies. The purpose of this paper is to further illuminate the causes of the variation of NBTI in deep submicron devices, already discussed in Refs. [2, 3].

Charging and discharging of individual oxide defects has been readily observable in sub-micron FETs in the form of random telegraph noise (RTN). Recently, threshold voltage steps due to individual defects were also observed in NBTI relaxation transients [3-6]. We have already argued in [4] that both effects are in fact but the two facets of the same mechanism, with RTN being the channel/gate dielectrics system in the state of dynamic equilibrium, while NBTI relaxation corresponding to the perturbed system returning to this equilibrium (Fig. 1) [7]. Here we will show that, identically to RTN amplitude distribution, the *individual* NBTI relaxation steps are exponentially distributed in amplitude [8]. The exponential distribution will be confirmed with a simplified percolation stochastic model. Combined with the assumption of the Poisson-distributed number of trapped gate oxide charges, an *analytical* description of the *total* NBTI threshold voltage shift distribution is then derived. This allows, among other things, linking its first two moments with the average number of defects per device.

Finally, we will argue that NBTI in future downscaled devices will be treated as a stochastic ensemble of individual defects, Poisson-distributed in number per device, with each defect described by its impact on the channel conduction discussed here and its capture and emission times [5, 9].

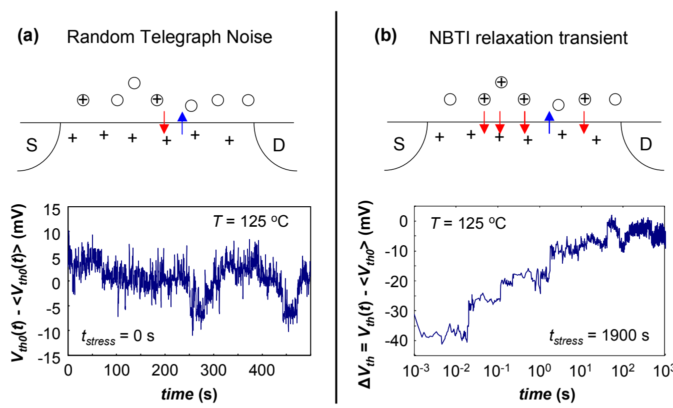

Figure 1. (a) At constant bias conditions, oxide defects are charged by channel carriers and subsequently discharged back into the channel with a wide range of time constants controlled by a nonradiative multiphonon emission process [9]. The system is in *dynamic* equilibrium, manifested by low-frequency noise or Random Telegraph Noise (RTN) in small devices. (b) Following the perturbation by NBTI stress, excess charged oxide defects gradually discharge and the system is returning to the dynamic equilibrium of (a), resulting in long NBTI transients.

This work is part of IMEC's Industrial Affiliation Program, funded by IMEC's core partners: Intel, Texas Instruments, Micron, Infineon, NXP, ST, Panasonic, TSMC, Samsung, and Elpida.

II. EXPERIMENTAL

pFETs with nominal gate length L = 70 nm (metallurgic length $L \sim 35$ nm), width W = 90 nm, and HfO_2 dielectrics with EOT = 0.8 nm were used in this study. Lanthanum has been incorporated in the oxide to boost the complementary nFET performance [10], but this was deemed to have no effect on the pFET NBTI [11] and especially on the NBTI variation discussed here.

All measurements were done at $T = 125\ ^{o}$C. To compensate for the variability of these aggressively scaled devices, the initial threshold voltage V_{th0} of each DUT was first automatically determined using a fixed I_S criterion. The DUT was then stressed at $V_G = V_{th0} - 1.2$V using the extended Measure-Stress-Measure (eMSM) sequence [12]. Specifically, the source current I_S in the linear regime (V_D = -0.1 V) was recorded during a series of 7 stress and relaxation phases. The relaxation phase I_S measured at $V_G \sim V_{th0}$ was converted to $V_{th}(t_{stress}, t_{relax})$ using the corresponding initial I_S-V_G curve. In our aggressively-scaled devices we estimate the V_{th} measurement accuracy to be ~1 mV. This is related to the relatively small current I_S at low V_G and V_D and to the conversion of I_S into V_{th} given the sub-threshold slope of our devices. Subsequently, ΔV_{th} was calculated as $\Delta V_{th} = V_{th}(t_{stress}, t_{relax}) - V_{th0}$. Note that because of the large RTN in the aggressively scaled devices, V_{th0} itself is not a fixed value, but rather fluctuates with time by up to ~10 mV, as shown in Fig. 1a. Consequently, it is possible to obtain small *positive* NBTI ΔV_{th} in a fraction of our devices, particularly for shorter stress times.

The resulting total threshold voltage shifts were found to be uncorrelated with the initial V_{th0} (Fig. 2), which confirmed that the NBTI mechanism is decoupled from sources of the V_{th0} variation and can be studied separately.

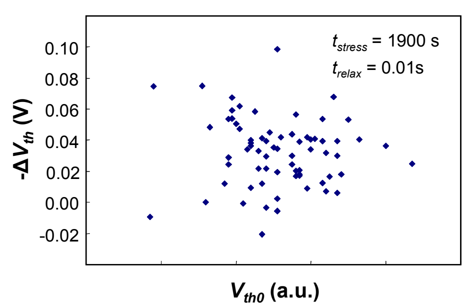

Figure 2. The lack of any correlation between the pFET initial threshold voltage V_{th0} and NBTI ΔV_{th} allows us to study the NBTI mechanisms independently of the pFET variation.

III. RESULTS

A. Observation of single discharge events

Fig. 3a shows a typical result of the MSM stress measurement. As already reported previously [3,4,6], clear steps caused by single discharge events are visible in the NBTI relaxation transients. However, the average step height is significantly larger than those reported earlier. A *single* discharging event in many devices routinely exceeded 15 mV, *and in several devices exceeded 30 mV*, the NBTI lifetime criterion presently used by some groups. For comparison, ΔV_{th} of less than 2 mV would be expected based on a simple charge sheet approximation. As will be shown below, the large observed step height amplitude is due to the aggressively scaled dimensions of the pFETs used.

The individual down-steps were detected in relaxation traces together with the corresponding relaxation times in all measured pFETs [9]. The step-detecting algorithm was designed to work automatically even in the presence of RTN in the traces. In order to ensure this, a detection resolution of 1 mV was used. Consequently, no steps smaller than 1 mV were detected.

An example of the result of this extraction is given in Fig. 3b. As already discussed previously [4], we did not observe any obvious correlation between the step height and trap emission time—all step heights appeared to be equally likely at all measured relaxation times in our 72 high-k pFETs. We have previously argued that this property is required in order to observe the long "featureless" log(t_{relax})-like relaxation tails [4]. This, however, also implies that defects exist with emission times faster than our measurement setup and we are therefore analyzing only the *visible*, but representative subset of all defects.

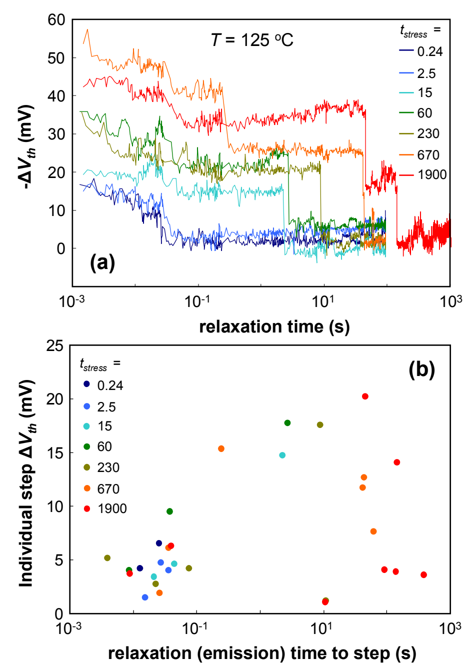

Figure 3. (a) A typical result of the eMSM sequence obtained on a single device: 7 NBTI relaxation transients following stress for the indicated times. Steps of varying heights due to single discharge events are clearly visible. (b) Step heights and the corresponding relaxation (emission) times for individual defects extracted from (a) [9].

B. Single discharge ΔV_{th} distribution

A histogram of the step heights from transients following the longest stress time is constructed from all 72 pFET devices in Fig. 4a. The figure shows that *the distribution of NBTI relaxation step heights is exponential,* with their probability distribution function (PDF) being

$$f_1(\Delta V_{th}, \eta) = \frac{1}{\eta} e^{-\frac{\Delta V_{th}}{\eta}}, \quad (1)$$

where the scaling factor η is the mean ΔV_{th} value for a *single* charge. The cumulative distribution function (CDF) corresponding to Eq. (1) is then

$$F_1(\Delta V_{th}, \eta) = 1 - e^{-\frac{\Delta V_{th}}{\eta}} \quad (2)$$

and the variance of this distribution is $\sigma^2 = \eta^2$. We note that the exponential distribution has been repeatedly reported for RTN amplitudes [13-15]. This similarity further strengthens the link shown in Fig. 1. We moreover note that the large range of possible ΔV_{th}'s gives each defect its *individual signature*, which e.g. allows tracing its properties under various stress conditions [5,6].

The maximum-likelihood fit to individual ΔV_{th}'s following the longest stress, shown in the *cumulative* plot in Fig. 4b, confirms the exponential distribution and allows extracting the average ΔV_{th} shift per single discharge η = 4.75±0.3 mV in our devices. An exponential distribution is also observed for shorter stress times, including the shortest t_{stress} shown in Fig. 4a, but given the amount of collected data we only *assume* it has the same η. We note that η varying with the stress time could indicate e.g. charging of defects at varying depths. This is not expected for the NBTI mechanism, which has been repeatedly shown to be occurring at or very close to the Si/SiO_2 interface [11]. This also agrees with the non-correlation between single ΔV_{th}'s and emission times discussed above.

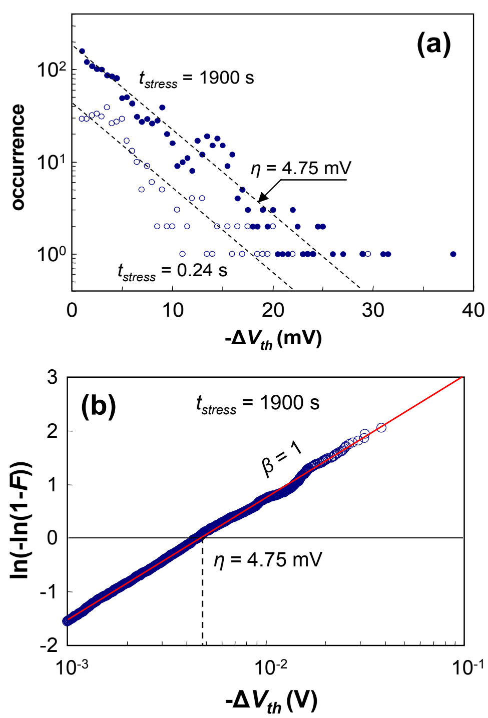

Figure 4. (a) Histograms of NBTI transient step heights for 72 devices show a clear exponential distribution. (b) CDF of the t_{stress} = 1900 s data in (a) shown in Weibull plot confirms exponential distribution (i.e., Weibull with shape factor β = 1).

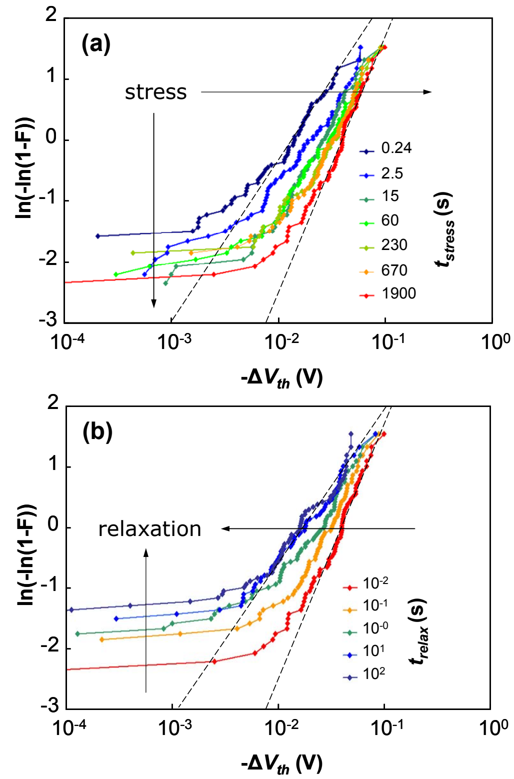

Figure 5. (a) Cumulative distribution of the total ΔV_{th} for 72 pFETs following stress at indicated stress times. With increasing t_{stress} the mean $\langle\Delta V_{th}\rangle$ increases, while the fraction of devices with negligible ΔV_{th} decreases. (b) Cumulative distribution of ΔV_{th} for the same devices during relaxation following the longest stress of 1900 s. The opposite trends are observed.

C. *Total ΔV_{th} distribution*

Fig. 5a shows the distribution of the *total* ΔV_{th} of 72 pFETs for increasing stress times, corresponding to an increasing number of charged defects. Such total ΔV_{th} distributions are typically reported for a particular technology [3]. In Fig. 5a we note that the mean and maximum ΔV_{th}'s are increasing with stress, its *relative* deviation is decreasing (the distribution is getting *relatively* tighter). Perhaps surprisingly, Fig. 5a also demonstrates that a fraction of devices exists with negligible ΔV_{th} even after the longest stress. Overall, this fraction decreases with increasing stress time, i.e., with increasing mean ΔV_{th}. The opposite trends are observed in Fig. 5b when the devices are left to relax after the longest stress.

IV. Discussion

As we will now show, all the trends as well as the total ΔV_{th} distribution itself, can be fully analytically described if i) the number of defects per device is assumed to follow a Poisson distribution, while ii) the impact of each individual defect on ΔV_{th} is exponentially distributed.

A. *Single discharge ΔV_{th} distribution*

The exponential distribution of single-charge ΔV_{th} can be understood if non-uniformities in the pFET channel due to random dopant fluctuations (RDF) are considered [13-15]. The threshold voltage of such a device corresponds to the formation of a conduction (percolation) path in the random dopant potential between Source and Drain (Fig. 6a). To zeroth order, depending on the position of the NBTI-stress-generated oxide charge, the conduction path could be either unaffected or obstructed by the new charged defect. In the latter case, the drop in the current has to be compensated by an increase of the gate voltage, resulting in the observed ΔV_{th}.

A.1. Simplified channel percolation model

An accurate reproduction of this process is typically done through computation-intensive physics-based device simulations with RDF, line edge roughness, and other realistic effects [15,16]. Here we show that the essence of the mechanism can be qualitatively captured in a very simplified channel percolation model. We emphasize that in contrast to the all-encompassing device simulations, our aim is to keep the model as simple as possible and to include only the bare minimum of assumptions. We find it very instructional that the minimalist model correctly reproduces most of the common observations.

In our simplified model (Fig. 6b), a mesh of "elementary" FETs with random V_{th}'s, representing variations in the local potential, is set up to represent the channel of our pFETs. For the sake of simplicity, a uniform distribution of the random "elementary" V_{th}'s is used and short-channel effects are not considered. A script is used to generate 400 instances of the randomized mesh, to call SPICE to solve them, and to extract the V_{th0} of the simulated pFET. As is typically experimentally observed, the resulting V_{th0}'s are normally distributed (Fig. 7a) and their variance scales reciprocally with the FET area (Fig. 7b).

A number n of "charged defects" is then inserted, each represented by an additional V_{th} shift of one random "elementary" FET in the netlist. A fixed value of V_{th} shift for these "single oxide charges" is assumed, representing the fact that NBTI charges are occurring very close to (i.e., at a fixed distance from) the substrate interface. Subsequently, a new V_{th} is calculated, resulting in ΔV_{th} for each pFET instance. For a single additional charged defect, the simplified model shows the ΔV_{th} distribution to be Weibull-distributed with $\beta = 0.8$ for a range of dimensions of the channel mesh (Fig. 8). This confirms that the above described process can be responsible for the observed exponential distribution of step heights (cf. Fig. 4b).

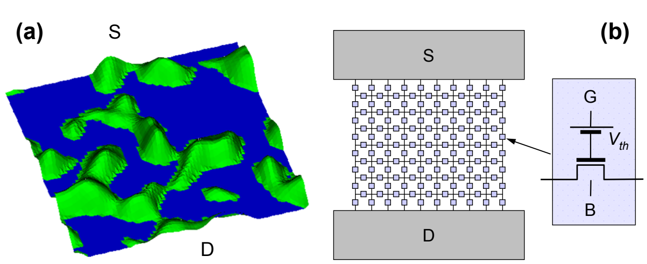

Figure 6. (a) An illustration of a percolation path in a random potential (from [17]) such as that between FET source and drain. (b) A mesh of "elementary" FETs with random V_{th}'s (voltage source in series with gate) representing (a) can be readily solved with SPICE.

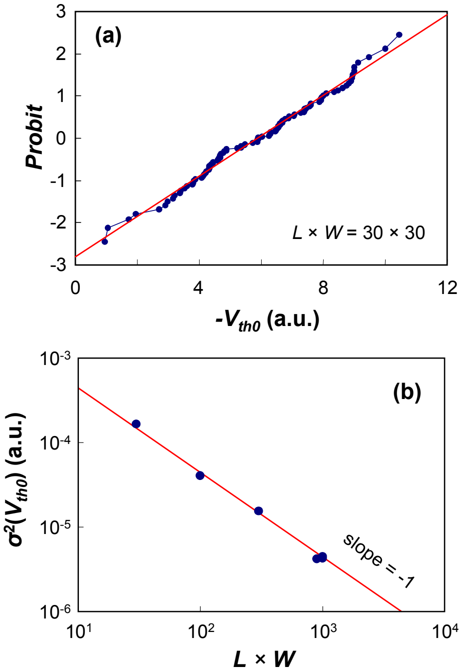

Figure 7. The simple percolation model correctly reproduces (a) the normal distribution of initial threshold voltages V_{th0} and (b) the variance σ^2 of V_{th0} scaling reciprocally with the $L \times W$ (Pelgrom's rule) [18].

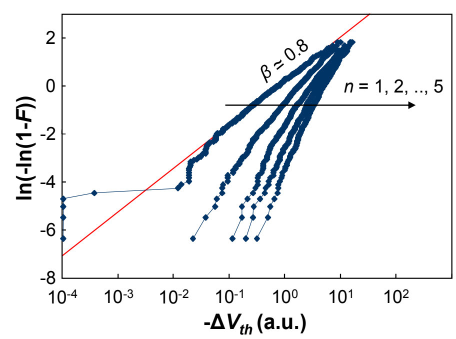

Figure 8. Cumulative ΔV_{th} distributions generated for an increasing number of gate oxide defects n by the simplified channel percolation model. For a single charged defect ($n = 1$), the model well reproduces the observed exponential distribution in Fig. 4b.

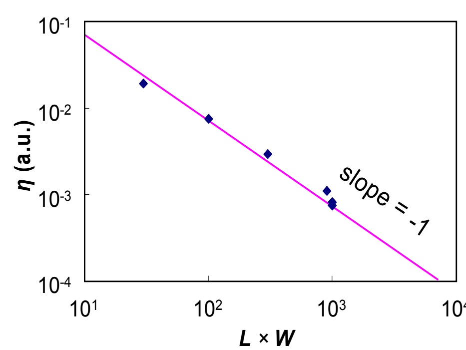

Figure 9. The step heights due to individual discharge events will increase with both decreasing L and W, explaining why large single-charge steps can be expected in very small devices.

The simplified model predicts that η scales inversely with both W and L (Fig. 9), i.e., the smaller the device the larger the steps, thus explaining the large observed value of η. This can be understood as the impact of a single charge relatively increasing as the device becomes smaller. We note here that a more thorough discussion of the dependence of η on W, L, EOT, and channel doping in the framework of RTN is given in Ref. [15], which infers $\eta \sim L^{-1/2}$ for short devices.

The simplified model also predicts the *total* ΔV_{th} distribution for the number of defects $n > 1$ (Fig. 8). Since the subsequent charge lateral locations are uncorrelated, the overall ΔV_{th} distribution can be readily expressed as a convolution of individual exponential distributions (Eq. 1), and the PDF and the CDF are respectively described by

$$f_n(\Delta V_{th},\eta) = \frac{e^{-\frac{\Delta V_{th}}{\eta}}}{(n-1)!}\frac{\Delta V_{th}^{\;n-1}}{\eta^n} \quad (3)$$

and

$$F_n(\Delta V_{th},\eta) = 1 - \frac{\Gamma(n,\Delta V_{th}/\eta)}{(n-1)!}. \quad (4)$$

The fraction in Eq. 4 can be also recognized as the regularized gamma function. CDF in Eq. 4 well describes the result in Fig. 8 for $\beta = 1$.

B. *Total ΔV_{th} distribution*

An actual population of stressed devices will consist of devices with a *different* number n of visible oxide defects in each device. That number will be Poisson distributed [2-4,16]. The *total* ΔV_{th} distribution can be therefore obtained by summing distributions F_n weighted by the Poisson probability

$$P_N(n) = \frac{e^{-N}N^n}{n!}. \quad (5)$$

In Eq. 5, N is the mean number of defects in the FET gate oxide and is related to the oxide trap (surface) density N_{ot} as $N = W\,L\,N_{ot}$ (note that N is not an integer).

This reasoning then results in the *total* ΔV_{th} CDF given by

$$F_N(\Delta V_{th},\eta) = \sum_{n=1}^{\infty}\frac{e^{-N}N^n}{n!}F_n(\Delta V_{th},\eta). \quad (6)$$

The corresponding PDF is

$$f_N(\Delta V_{th},\eta) = e^{-N}\left[\delta(\Delta V_{th}) + N\frac{e^{-\frac{\Delta V_{th}}{\eta}}}{\eta}\,{}_0\mathcal{F}_1(2;N\frac{\Delta V_{th}}{\eta})\right], \quad (7)$$

where the hypergeometric function ${}_0\mathcal{F}_1(2;x)$ can be also written in terms of the modified Bessel function I_1 as ${}_0F_1(2;x) = x^{-1/2}I_1(2x^{1/2})$. The Dirac $\delta(\Delta V_{th})$ term represents the fraction of devices with 0 V shift [14], which decreases with increasing N.

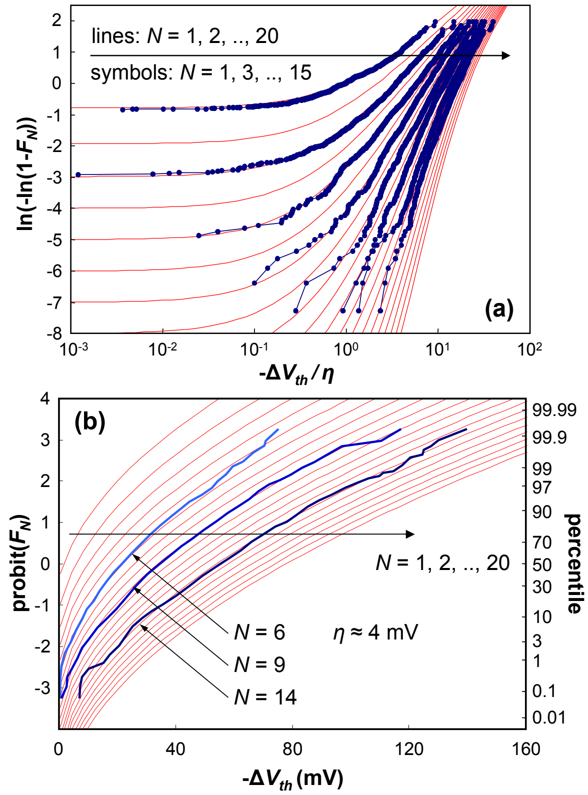

Figure 10. Eq. 6 for several values of the average number of defects N (lines). (a) Weibull plot emphasizes the fraction of devices with $\Delta V_{th} \sim 0$ V, cf. Fig. 5. Monte Carlo calculation with 1000 samples is included for comparison (symbols). (b) Eq. 6 in a probit plot rescaled to fit experimental distributions from Fig. 10 of Ref. [3], with the corresponding values of N and η readily extracted.

The CDF of Eq. 6 is plotted in Fig. 10 for several values of N. We can see that it has the same properties as the distributions obtained on the limited population in Fig. 5; specifically, the fraction of devices showing negligible ΔV_{th} varies with $\langle\Delta V_{th}\rangle$. For completeness, the CDF is also compared with a simple, 1000-sample Monte Carlo calculation assuming i) exponentially distributed individual ΔV_{th} steps ii) Poisson-distributed in number (Fig.10a). Fig. 10b then shows Eq. 6 in a probit plot, such as that used in Refs. [2,3,16]. For comparison, measured total ΔV_{th} distributions from Ref. [3] are excellently fitted by Eq. 6, which further supports our assumptions above.

C. *Implications*

The advantages of describing the total ΔV_{th} distribution in terms of Eqs. 6 and 7 are their relative simplicity and tangibility of the variables, while the analytical description allows further statistical treatment. The mean of the above-derived distribution is

$$\langle\Delta V_{th}\rangle = N\eta, \quad (8)$$

i.e., it should be independent of FET gate area $L\times W$ provided N and η are respectively directly and inversely proportional to $L\times W$. The variance of the distribution is then

$$\sigma^2_{\Delta Vth} = 2N\eta^2, \tag{9}$$

i.e., it increases with decreasing gate area. The relative deviation $\sigma_{\Delta Vth}/\langle V_{th}\rangle = (2N)^{-1/2}$ is therefore decreasing with increasing N, as observed in Fig. 5.

With the value of η extracted from the single discharge step height histogram in Fig. 2 earlier, we can use Eq. 8 to convert $\langle\Delta V_{th}\rangle$ to the average number of trapped defects N. In our devices, N increases from 2.6 (t_{stress} = 0.24 s, Fig. 1) to 6.9 (t_{stress} = 1900 s), and then decreases to 3.4 (t_{relax} = 10 s). These values correspond to effective trap densities of 1-2×10^11^ cm^-2^, typically observed for NBTI in large devices.

We acknowledge that obtaining the value of η as in Fig. 2 could be rather laborious. Eqs. 8 and 9, however, allow us expressing both N and η in terms of $\langle\Delta V_{th}\rangle$ and $\sigma^2_{\Delta Vth}$ as

$$N = \frac{2\langle\Delta V_{th}\rangle^2}{\sigma^2_{\Delta Vth}} \tag{10}$$

and

$$\eta = \frac{\sigma^2_{\Delta Vth}}{2\langle\Delta V_{th}\rangle}. \tag{11}$$

This means that both N and η can be extracted from the first two moments of a measured total NBTI distribution, *without having to characterize individual step heights*. This way we *independently* obtain N increasing from 1.9 to 4.6 with stress and η varying between 7 and 9 mV. For the limited population of devices measured, these values are very close to those obtained directly by counting individual ΔV_{th} step heights in Fig. 4. Note that other effects potentially increasing $\sigma_{\Delta Vth}$, such as the variance of the initial V_{th0} (Fig. 1a) and FET variability (line-edge roughness, work-function fluctuations, etc.) have not been considered here.

D. Reliability projection of future downscaled devices

Finally, we review the described concepts to illustrate the paradigm shift in understanding NBTI reliability in aggressively scaled devices. Fig. 11a illustrates the reliability projection in large devices of the past. Since all devices are expected to behave identically, there is no device-to-device variation. Measuring and extrapolating one stress condition per device is therefore sufficient. Additionally, there is also the application-independent hard failure criterion.

In contrast to that, future failure criteria will be application-dependent and will depend specifically on the circuit immediately surrounding the device in question. Each deca-nanometer device will be described by the Poisson-distributed total number of defects, each of which is characterized by i) voltage and temperature dependent capture time τ_c and ii) emission time τ_e, and iii) its impact on the FET current (e.g. via ΔV_{th}). This is schematically illustrated in Fig. 11b. The PDFs of all three parameters are known: i) and ii) appear to be uniform on the log scale (at least within the measured ~10^-6^ – 10^6^ s range so far) [12]. In this description, "permanent" defects can be seen as those with $\tau_e \sim \infty$. Significant progress in describing the voltage and temperature dependence of τ_c and τ_e using nonradiative multiphonon theory has been made [9]. The exponential PDF of iii) has been justified here. Fig. 11c then schematically summarizes the progress of NBTI in the three hypothetical devices shown in Fig. 11b. For simplicity, only continuous stress is illustrated, although the specified parameters for each device (Fig. 11b) allow evaluating the degradation following an arbitrary waveform [5]. The origin of the NBTI variability at a given time or a given ΔV_{th} is apparent.

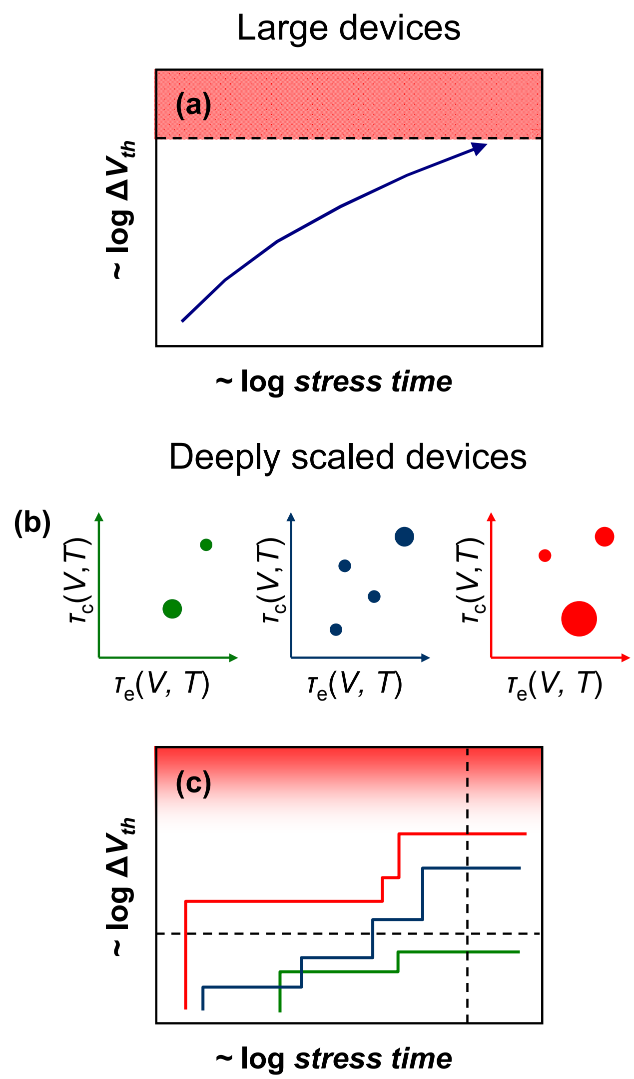

Figure 11. (a) All large devices behave identically upon stress and are expected to fail when reaching the projected "hard" degradation criterion. (b) NBTI degradation in deeply scaled devices can be described in terms of the total number of defects in each device, their (voltage and temperature dependent) capture and emission times, and their impact on the device (demarked by the size of the point). (c) Schematic showing the progress of stress in the three devices described in (b). The origin of the NBTI variability is apparent.

V. CONCLUSIONS

The correspondence between RTN and NBTI relaxation was further strengthened by our observation of exponentially distributed step heights in NBTI transients in deeply scaled pFETs. A simplified channel percolation model was devised to illustrate and to confirm this behavior. The overall ΔV_{th} distribution was argued to be a convolution of exponential distributions of uncorrelated individual charged defects. The analytical description derived for this distribution should prove useful for both reliability data analysis and simulations of deeply-scaled CMOS circuitry. The proposed picture allows us to predict that the reliability of future deca-nanometer devices will be treated as a stochastic ensemble of the Poisson-distributed total number of defects, each characterized by capture and emission times and its impact on the FET current.

REFERENCES

[1] R. Degraeve, G. Groeseneken, R. Bellens, M. Depas, and H. E. Maes, "A consistent model for the thickness dependence of intrinsic breakdown in ultra-thin oxides," *Int. Electron Devices Meeting Tech. Dig.*, pp. 863 – 866, 1995.

[2] S. E. Rauch, "Review and Reexamination of Reliability Effects Related to NBTI Statistical Variations", *IEEE T. Dev. Mat. Rel.* **7**, p. 524, 2007.

[3] V. Huard C. Parthasarathy, C. Guerin, T. Valentin, E. Pion, M. Mammasse, N. Planes, L. Camus, "NBTI degradation: From Transistor to SRAM Arrays," *Proc. Int. Rel. Phys. Symp.*, p. 289, 2008.

[4] B. Kaczer, T. Grasser, J. Martin-Martinez, E. Simoen, M. Aoulaiche, Ph. J. Roussel, and G. Groeseneken, "NBTI from the Perspective of Defect States with Widely Distributed Times," *Proc. Int. Rel. Phys. Symp.*, p. 55, 2009.

[5] H. Reisinger, T. Grasser, W. Gustin, and C. Schlünder, "The Statistical Analysis of Individual Defects Constituting NBTI and its Implications for Modeling DC- and AC-Stress," presented at *Int. Reliab. Phys. Symp.*, 2010.

[6] T. Grasser, H. Reisinger, W. Goes, Th. Aichinger, Ph. Hehenberger, P.-J. Wagner, M. Nelhiebel, J. Franco, and B. Kaczer, "Switching Oxide Traps as the Missing Link Between Negative Bias Temperature Instability and Random Telegraph Noise, " *Int. Electron Devices Meeting Tech. Dig.*, pp. 729-732, 2009.

[7] A. Karwath and M. Schulz, "Deep level transient spectroscopy on single, isolated interface traps in field-effect transistors", *Appl. Phys. Lett.* **52**, pp. 634-636, 1988.

[8] B. Kaczer, Ph. J. Roussel, T. Grasser, and G. Groeseneken, "Statistics of multiple trapped charges in the gate oxide of deeply-scaled MOSFET devices—application to NBTI," accepted to *Electron Dev. Lett.*

[9] T. Grasser, H. Reisinger, P.-J. Wagner, F. Schanovsky, W. Goes, and B. Kaczer, "The Time Dependent Defect Spectroscopy (TDDS) for the Characterization of the Bias Temperature Instability", presented at *Int. Reliab. Phys. Symp.*, 2010.

[10] L.-Å. Ragnarsson, Z. Li, J. Tseng, T. Schram, E. Rohr, M. J. Cho, T. Kauerauf, T. Conard, Y. Okuno, B. Parvais, P. Absil, S. Biesemans, and T. Y. Hoffmann, "Ultra Low-EOT (5 Å) Gate-First and Gate-Last High Performance CMOS Achieved by Gate-Electrode Optimization", *Int. Electron Devices Meeting Tech. Dig.*, pp. 663-666, 2009.

[11] B. Kaczer, A. Veloso, Ph. J. Roussel, T. Grasser, and G. Groeseneken, "Investigation of Bias-Temperature Instability in work-function-tuned high-k/metal-gate stacks", *J. Vac. Sci. Technol. B* **27**, pp. 459-462, 2009.

[12] B. Kaczer, T. Grasser, Ph. J. Rousse, J. Martin-Martinez, R. O'Connor, B. J. O'Sullivan, and G. Groeseneken, "Ubiquitous Relaxation in BTI stressing—New Evaluation and Insights", *Proc. Int. Reliab. Phys. Symp.*, p. 20, 2008.

[13] A. Asenov, R. Balasubramaniam, A. R. Brown, and J. H. Davies, "RTS Amplitudes in Decananometer MOSFETs: 3-D Simulation Study," *IEEE T. Electron Dev.*, vol. 50, no. 3, p. 839, 2003.

[14] K. Takeuchi, T. Nagumo, S. Yokogawa, K. Imai, and Y. Hayashi, "Single-Charge-Based Modeling of Transistor Fluctuations Based on Statistical Measurement of RTN Amplitude," *Symp. VLSI Tech.*, p. 54, 2009.

[15] A. Ghetti, C. M. Compagnoni, A. S. Spinelli, and A. Visconti, "Comprehensive Analysis of Random Telegraph Noise Instability and Its Scaling in Deca–Nanometer Flash Memories," *IEEE T. Electron Dev.*, vol. 56, no. 8, pp. 1746-1752, 2009.

[16] M. F. Bukhori, S. Roy, A. Asenov, "Simulation of statistical aspects of reliability in nano CMOS," presented at *Int. Integ. Rel. Workshop,* 2009.

[17] http://www.ibiblio.org/e-notes/Perc/contour.htm .

[18] M. J. M. Pelgrom, A. C. J. Duinmaijer, and A, P. G. Welbers, "Matching Properties of MOS Transistors", IEEE J. Solid-State Circ. **24**, pp. 1433-1440, 1989.